13

# The features of the proton exchange process during the formation of planar waveguides on lithium niobate crystals in the presence of thermogravitational convection

© A.I. Gordeeva, M.I. Petukhov, I.V. Petukhov, A.R. Kornilicyn, E.V. Myasnikova, D.N. Masalkin

Perm State University,
614990 Perm, Russia
e-mail: gordeeva@psu.ru

*Received January 12, 2025*
*Revised September 18, 2025*
*Accepted October 20, 2025*

The experimental work has studied the effect of thermogravitational convection on the depth and phase composition of planar waveguides formed on crystals of lithium niobate during proton exchange. The properties of the waveguides were determined using structural and optical methods. The impact of hydrodynamic flows was assessed by counting the number of protons penetrating into the crystal. It has been experimentally demonstrated that the presence of convective flows positively affects the rate of proton exchange. The reduction in the thickness of the layer with an increased concentration of lithium ions, which forms in the acid melt at the surface of the crystal, may be one of the proposed reasons for the observed effect.

**Keywords:** integrated optical phase modulator, proton exchange, thermogravitational convection, lithium niobate, planar waveguide.

DOI: 10.61011/TP.2026.01.62854.4-25

## Introduction

Presently, the whole world is involved in intensely designing and producing high-precision sensors and monitoring system with extended operating properties. Some of basic elements of these devices are phase modulators that are also widely used in fiber-optic communication lines, along which the major part of data is transmitted today [1–6]. Components of integral and fiber optics are widely used in science and technology [7–11]. Most often, assembly of the modulators includes channel waveguides, whose quality determines accuracy and efficiency of operation of optoelectronic instruments. Planar waveguides are also in great demand, since they are characterized by stable parameters with a wide range of variation of the optical properties. Gradient planar waveguides are manufactured by ion implantation methods [12], effusion [13], solid-state [14] and electrostimulated diffusion [15] and by means of ion exchange [16,17].

Most often, when the waveguides are manufactured by the ion exchange method, lithium niobate crystals ($LiNbO_3$) [18,19] are used, and on their surface ions are substituted with donor atoms of salts and acids. From appearance of a proton exchange technology, the main efforts have been directed at designing methods that would allow producing the waveguides with a predefined phase composition [20–22]. As shown in the studies [20–26], inside a the crystal proton exchange can result in formation of separate submicron-thick sublayers with mutually different crystal phases, whose formation depends on parameters such as crystal-lattice orientation of a substrate, a rate and temperature of the process, etc.Seven different crystal phases of $H_xLi_{1-x}NbO_3$ were identified in total. The studies [23–26] have experimentally determined a crystal structure, refractive index, proton concentration and ferroelectric properties of the layers in a dependence on a type of the phase formed in the waveguide. As shown in the studies [27,28], deep protonation degrades electrooptical properties of the waveguide layer, thereby resulting in high losses and instability of the waveguide parameters over time. Melt buffering, annealing and other methods of stabilization of a proton concentration make it possible to eliminate the said drawbacks [29–33].

All the above-described studies are dedicated to investigating formation of optical phases, but they do not describe a behavior of melts of salts or acids that are involved in the proton exchange process. Proton exchange is a surface process that proceeds in a thin "melt-crystal" layer, whose rate depends not only on a rate of ion diffusion in a sample, but on a rate of ion supply from a melt volume to the sample surface and their removal from exchange locations. Theoretical studies [34,35] have shown that during exchange of lithium ions with benzoic acid protons a boundary ion layer is formed near the crystal surface. Products of a proton exchange reaction, namely, the lithium ions and benzoate ions recombine, thereby resulting in origination of a lithium benzoate impurity in the melt. In turn, it presence can cause reduction of the protonation rate [33]. Potentially, a thickness of the boundary layer can be controlled by creating thermogravitational convection or thermoelectric convection in a reactor, affecting by flows stratification of horizontal layers that slightly mix with each other. A typical

value of the thermal expansion coefficient $\beta$ of benzoic acid at the temperature of 473 K is $1.14 \cdot 10^{-3}$ 1/K and surface tension's temperature heterogeneity $\sigma_T$ is estimated to be $9 \cdot 10^{-5}$ N/(m·K) [36,37]. The high values of $\beta$ and $\sigma_T$ indicate that the acid melt is sensitive to temperature drops. Even the small gradient of $T$ in the reactor when heating it up at a side will result in excitation of a convective flow that initiates active mass transfer [38,39]. The studies [40,41] clearly demonstrate an effect of influence of thermo- and concentrationally-capillary convection on a shape and intensity of bulk fluxes. These tasks must take into account an action of Marangoni surface forces that largely affect motion of a liquid in the volume.

As a rule, the protonation process proceeds in a tightly closed reactor arranged in a isolated thermal chamber, in which the system is heated as per a pre-defined program of heating, holding and cooling with stabilization of an operating temperature of $\pm 1$ K. It is assumed that in this situation the reactor's internal volume is uniformly heated and the system has not large-scale convective fluxes. Inhomogeneous heating of the walls or a bottom of the reactor can result in formation of the temperature gradient, which will, in turn, excite thermogravitational convection in the benzoic acid melt [38,42–46]. Presence of a washing flow can prevent accumulation of lithium benzoate near the crystal surface, which, in turn, also affects a rate of formation of an proton-exchange layer.

In order to check a hypothesis of formation of the boundary ion layer, the present study has experimentally checked the effect of thermogravitational flow that is excited in the benzoic acid melt when inhomogeneously heating the reactor bottom, on optical characteristics of the planar waveguides that are formed on the lithium niobate crystals during two-hour exchange at the process's average temperature of 463 K. In order to estimate typical rates of convective mass transfer in the benzoic acid melt, the present study has numerically simulated a problem in a two-dimensional formulation.

The performed research requires deep understanding of processes that proceed at an interphase boundary of reacting media. The studies in this field are at the junction of two scientific fields — physical chemistry and hydrodynamics. Difficulties that arise when studying multi-phase systems require complex investigation of the process both theoretically and experimentally. In this case an experiment will well verify the theoretical model, while the theory will provide deeper understanding of the processes and mechanisms that proceed in the experiment.

## 1. Materials and methods of experimental study

The effect of the thermogravitational flow on the characteristics of the planar waveguides that are formed on the lithium niobate crystals *1* during proton exchange when they contact the benzoic acid melt *2* was experimentally studied (Fig. 1) in the titanium reactor *3* AN-0034 manufactured by LLC „Kontsept-Lab" (Moscow). An internal volume of the reactor was a cylinder of the diameter of 50 mm and the height of 20 mm. Temperature measurement and estimation of intensity of the convective flow in the acid melt was conducted by means of six thermocouples input into the reactor via an L-shaped tube of the diameter of 6 mm, which was coupled to an upper bowl. After the thermocouples were input, prior to proton exchange, a working hole was treated with a temperature sealant for cutting off the internal volume of the reactor from an external medium.

The thermocouples of two chromel-alumel threads were manufactured by carbon welding without using a solder. In order to protect against oxidation, the threads were drawn through PTFE tubes, whose butt ends were treated with a chemically-resistant high-temperature sealant Permatex (USA). Inside the reactor, the thermocouples were fixed at a pre-defined distance from each other by means of an aluminum plate that did not contact the acid during proton exchange. A different position of the thermocouples relative to a reactor center made it possible to judge intensity and a structure of the flow washing the crystal surface. Besides, studies by means of additional thermocouples included measurement of the temperature of a gas phase inside the thermal chamber. Readings of the temperatures were recorded in real time to a personal computer by means of a multi-channel recorder with accuracy $\pm 0.05$ K.

In order to select a proton exchange mode realized in the titanium reactor under effect of the washing flow, the study included experiments with temperature control in three different variations. Depending on an executed cycle, the acid-filled reactor was placed either into an isolated thermal chamber, which is a classical method for proton exchange, or, to the surface of an energy source with a constant heat-release density to create convection in the melt. For more local heating, the reactor was installed to a copper cylinder *4* of the diameter of 30 mm and the height of 20 mm. The reactor position in relation to a heat source center made it possible not only to adjust a value of the maximum temperature drop, but to pre-define a shape of a convective vortex as well.

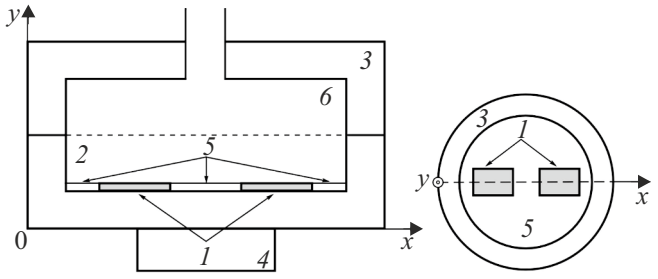



**Figure 1.** Geometry of the system: a side view in the middle section (on the left), a plan view of the reactor's lower bowl (on the right), *1* — the lithium niobate crystals, *2* — the benzoic acid melt, *3* — the titanium reactor, *4* — the heater, *5* — the aluminum mask, *6* — benzoic acid vapor.

During proton exchange in the thermal chamber, the L-shaped tube was inside it for 90 % of its length. During the experiments using the surface energy source, the entire structure was in direct contact with the air medium of a working room. In this formulation of the experiment, it can be assumed that the observed temperature gradients in the acid melt are not related to a specific feature of the reactor structure, but rather induced by presence of external temperature drops.

The temperature was detected during proton exchange in the thermal chamber to show that the internal volume of the reactor was heated more slowly than a heating rate pre-defined by a controller program. In the studied heating mode at the rate of 3 K/min to $T = 463$ K the samples shall be at the temperature of $T = 463$ K for 2 h and then be cooled at the rate of 0.6 K/min. But the benzoic acid was at the temperature pre-defined by the mode for 1 h instead of two pre-defined ones. The recorded time and temperature differences demonstrate that is necessary to actually measure the temperature when changing materials and dimensions of the reactor as well as conditions for proton exchange. Thus, replacing the zirconium reactor with the thermal conductivity coefficient $\lambda = 21.4$ W/(m·K) at 500 K with the titanium one with $\lambda = 19.7$ W/(m·K) at 500 K [47] can change a pace of acid heating and result in variations of the characteristics of the waveguides being manufactured. One's own contribution can be made by a variation of wall thicknesses and the reactor bowl geometry. In our case, the temperature measurement was a prerequisite for the experiment to further verify and compare data obtained at the various proton-exchange cycles. In order to correct a growth pace and two-hour holding of the acid volume at the required temperature $T = 463$ K during proton exchange in the thermal chamber, the study included pre-defining the cycle of heating at 4.5 K/min to $T = 493$ K, holding at $T = 493$ K for 16 min, $T = 463$ K for2 h and cooling at 0.6 K/min.

A capability of temperature measurement during the process cycle made it possible to select programs for proton exchange realized using the surface energy source with the constant heat-release density, with the similar pace of heating, holding and cooling the internal volume of the reactor during proton exchange in a closed space of the thermal chamber. At the same time, the reactor bottom was locally heated to create the temperature drop up to $\Delta T = 0.5$ K/cm while maintaining the average temperature of 463 K.

The study included proton exchange on the surface of the bulk lithium niobate samples of *Z*- and *X*-transects of the thickness $h = 1$ mm. The samples of the size $10 \times 15$ mm were produced by disc cutting of a Fomos-produced substrate with a roughness degree $R_a < 1$ nm. Before the experiment, all the samples were washed in dimethyl-sulfoxide and isopropyl alcohol ($T = (296 \pm 0.5)$ K) using an ultra-sound bath for 5 min in each substance. After cleaning, the crystals were placed to the reactor bottom and covered with a uniform layer of crushed benzoic acid dried by holding it in a desiccator with calcined $CaCl_2$. The characteristics of the produced waveguides were studied to show that the optical properties significantly depend on an initial position of the crystals inside the reactor. They were fixed by placing an aluminum mask *5* (Fig. 1) of the thickness of 0.8 mm to the bottom, which had sample holes that were symmetrically arranged relative to the systems center. Fixation of the samples makes it possible to prevent their displacement along the reactor bottom when it is filled and to compare in the future detected heterogeneities of the proton-exchange layer along the crystal surface with the shape and intensity of convective torrents. In order to estimate the phase composition of the proton-exchange waveguides, the produced crystals were studied by X-ray diffraction analysis (XDA) in an X-ray double-crystal diffractometer DRON-UM1 (Russia). A monochromator was a silicon single crystal without dislocations, which was installed in a position of reflection of the $K_\beta$-line of Co radiation (the wavelength $\lambda = 1.62075$ Å) from the lattice plane (111). All the measurements were at the room temperature $T = (296 \pm 0.5)$ K. In order to limit dimensions of an X-ray beam, two slits were installed downstream of the crystal monochromator: a vertical one of the size of 1.0 mm and a horizontal one of the size of 0.2 mm. A vertical slit of the width of 0.05 mm was installed upstream of a counter. The XDA method allows determining integral intensity of the beam $I$ in a dependence on an orientation angle $\theta$.

Using the Bragg–Wulff condition

$$2d \cdot \sin\theta = n\lambda,$$

for a crystal's interplanar spacing $d$ in the manufactured samples a direction of elastic scattering diffraction maximums was calculated when $n = 1$. For qualitative comparison of the results, the integral intensity was normalized to the maximum value $I_{\max}$ and a dependence of the magnitude $I/I_{\max}$ on strain $\varepsilon = \Delta d/d$ was constructed. The obtained dependences were decomposed into separate peaks using the Fityk software. It was followed by determining types of the phases formed on the crystal surfaces based on structure-phase diagrams of the proton-exchange waveguide layers [26]. In order to estimate homogeneity of the characteristics of the experimental samples over the surface, the study included XDA determination of the phase composition of the proton-exchange waveguides in five different points. In addition to the point in the center, the integral intensity was additionally measured at the distance of 1 mm from an edge of the samples in the middle of their facets.

An increment of unusual beam's refractive index $\Delta n_e$ was experimentally measured on the samples by a method of prismatic input. A measurement technique is based on excitation of waveguide modes, which were input in the study by using a bismuth germanate prism and a laser with the radiation wavelength of $\lambda = 633$ nm. The increment of unusual beam's refractive index $\Delta n_e$ was determined by a Wentzel–Kramers–Brillouin method. The study [48]

describes a numerical method, which provides the same accuracy of reconstructing a refractive index profile of the diffusion waveguides of both a parabolic and an exponential type. From three to four orders of the waveguide modes were fixed in the studies described by us after proton exchange at the wavelength of 633 nm. And from six to eight orders thereof were recorded after a post-annealing procedure. This number of the modes make it possible to quite precisely reconstruct the refractive index profile of the waveguide and determine its depth $\delta$. A function $\Delta n_e$ was approximated in the MatLab software program by an algorithm specified in the study [48]. According to the study [26], when the waveguide includes at least two beta-phases, the increment of unusual beam's refractive index nonlinearly depends on the proton concentration in the phases. However, due to narrowness of their existence, when restoring the profile $\Delta n_e$ on $\delta$ in the first approximation one can use a linear dependence of $n_e$ on the proton concentration.

After determining the optical properties, the crystals were annealed at the temperature of 643 K in the dry atmosphere for 5 h and were studied again by means of XDA and mode spectroscopy. If there were still kappa-phases detected in the waveguide after annealing, the samples were annealed up in stages until their complete disappearance.

## 2. Numerical solution of the simulation problem

In addition to the full-scale experiments, the present study also included numerical simulation of convection of the benzoic acid melt in the two-dimensional formulation [42,49]. It allows estimating rates of convective transfer and demonstrating the structure of the flow that is formed in the benzoic acid melt when inhomogeneously heating the reactor bottom. The problem geometry is shown in Fig. 2.

When the problem is numerically solved, an upper boundary of the melt *1* is considered to be free and unstrained. It can be assumed since when taking into account a layer height $h = 8 \cdot 10^{-3}$ m under the gravitational acceleration $g = 9.8\,\mathrm{m/s^2}$ and with the characteristics of benzoic acid $\nu = 5.89 \cdot 10^{-7}\,\mathrm{m^2/s}$ — kinematic viscosity,

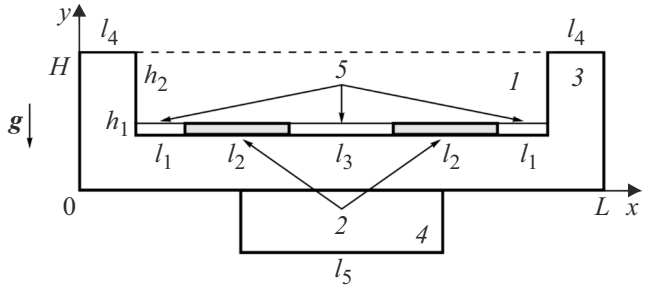



**Figure 2.** Problem geometry: *1* — the benzoic acid melt, *2* — the lithium niobate crystals, *3* — the titanium reactor, *4* — the heater, *5* — the aluminum mask.

$\chi = 6.1 \cdot 10^{-8}\,\mathrm{m^2/s}$ — thermal diffusivity, which are taken at the temperature of 463 K, a gravitational parameter $\mu = \nu\chi/gh^3$ is $7 \cdot 10^{-9}$ [36,37]. According to the study [38], irrespective of the value of surface tension, the liquid boundary can be considered to be flat when the values $\mu < 10^{-3}$. At the lower boundary, the melt *1* contacts the lithium niobate crystals *2*. Below and at the edges, the „melt-samples" system borders with walls of a heat-conducting array of the titanium reactor *3*. The system was heated by transfer of heat from the heater *4* and the reactor's external wall. A heat flux was described by means of thermal conductivity equations. Convective transfer in the benzoic acid melt when reaching the temperature of 463 K was described by Navier–Stokes equations in the Boussinesq approximation. It was simulated for two cases: with the aluminum mask *5* and without it.

Thus, the heat- and mass-transfer processes in the reactor can be described by the following system of equations [38,50]:

$$\frac{\partial \mathbf{v}}{\partial t} + (\mathbf{v}\nabla)\mathbf{v} = -\frac{1}{\rho_1}\nabla p + \nu\Delta\mathbf{v} + \mathbf{g}\beta(T_1 - T_m)f(t), \quad (1)$$

$$\rho_1 c_{p1}\left(\frac{\partial T_1}{\partial t} + (\mathbf{v}\nabla)T_1\right) = \lambda_1 \Delta T_1, \quad (2)$$

$$\rho_1 c_{pi}\frac{\partial T_i}{\partial t} = \lambda_i \Delta T_i, \quad (3)$$

$$\mathrm{div}\,\mathbf{v} = 0, \quad (4)$$

where $\mathbf{v}$, $T_1$, $p$ are fields of the rate, temperature and pressure in the melt; $\rho$, $\beta$, $\lambda$, $\nu$, $c_p$ — a density, the thermal expansion coefficient, thermal conductivity, kinematic viscosity and heat capacity at the constant pressure. $T_m$ and $\mathbf{g}$ are the melting temperature of benzoic acid and a gravitational acceleration vector directed against the axis $y$. Values of the index $i$ correspond to numbering of the arrays, which is shown in Fig. 2.

The melt borders solid walls of the arrays, at which the rate values were assumed to be zero: $\mathbf{v}|_B = 0$. In turn, the free boundary rate was determined via tangential stresses that are related to a dependence of surface tension on the temperature [38,51]:

$$y = H: \quad \eta\frac{\partial U_x}{\partial y} = -\sigma_T\frac{\partial T_1}{\partial x}f(t), \quad (5)$$

where $\eta = \nu\rho_1$ and $\sigma_T$ is dynamic viscosity and a coefficient that determines surface tension's temperature heterogeneity.

When calculating the fields of the temperature, the fourth-order conditions were set at all the internal boundaries:

$$\lambda_i\frac{\partial T_i}{\partial n} = \lambda_j\frac{\partial T_j}{\partial n}, \; T_i = T_j. \quad (6)$$

The upper boundaries of the area *2* had the thermal insulation condition $\partial T_1/\partial y = 0$ set. The other external boundaries had the heat transfer condition set:

$$\lambda_i\frac{\partial T_i}{\partial n} = \frac{\lambda_0}{h}(T_0 - T_i), \quad (7)$$

where $\lambda_0$, $T_0$ and $h$ are thermal conductivity and the temperature of air as well as a typical size of the space, into which heat is released. In the area where the reactor and the heater contact each other, the temperature was fixed: $T = T_h$.

A boundary value problem (1)–(7) was solved using the mathematical software package Comsol Multiphysics 6.1. The problem was solved using the MUMPS algorithm (MUltifrontal Massively Parallel sparse direct Solver). When solving, an uneven computational grid was generated, whose elements were condensed near boundaries of computational areas. Totally, the grid included the 350 000 elements.

## 3. Results and their discussion

When solving the boundary value problem (1)–(7), the following values of governing parameters were used:

$$\rho_1 = 1050\,\text{kg/m}^3,\ \rho_2 = 4640\,\text{kg/m}^3,\ \rho_3 = 4540\,\text{kg/m}^3,$$

$$\rho_5 = 2712\,\text{kg/m}^3,\ \beta = 10^{-3}\,\text{1/K},\ \nu = 10^{-6}\,\text{m62/s},$$

$$c_{p1} = 2000\,\text{J/(kg·K)},\ c_{p2} = 627\,\text{J/(kg·K)},$$

$$c_{p3} = 523\,\text{J/(kg·K)},\ c_{p5} = 897\,\text{J/(kg·K)},$$

$$\lambda_1 = 0.15\,\text{W/(m·K)},\ \lambda_2 = 40\,\text{W/(m·K)},\ \lambda_3 = 21.9\,\text{W/(m·K)},$$

$$\lambda_5 = 237\,\text{W/(m·K)},\ \lambda_0 = 0.03\,\text{W/(m·K)},$$

$$T_m = 396\,\text{K},\ T_h = 398\,\text{K},\ \sigma_T = 9 \cdot 10^{-5}\,\text{N/(m·K)},$$

$g = 10\,\text{m/s}^2$ [36,37,52]. At the free boundary $T_0 = 396\,\text{K}$, $h = 0.01\,\text{m}$. At the other external boundaries $T_0 = 293\,\text{K}$, $h = 0.1\,\text{m}$. At the initial moment of time, the temperature in all the areas was assumed to be 293 K, while the rate in the area *1* was zero. The system dimensions were pre-defined as follows: $L = 0.055\,\text{m}$, $H = 0.015\,\text{m}$, $h_1 = 0.001\,\text{m}$, $h_2 = 0.014\,\text{m}$, $l_1 = 0.005\,\text{m}$, $l_2 = 0.015\,\text{m}$, $l_3 = 0.01\,\text{m}$, $l_4 = 0.005\,\text{m}$, $l_5 = 0.015\,\text{m}$.

As mentioned above, the magnitudes $\beta$ and $\sigma_T$ have quite high values, which potentially lead to numerical instability. Therefore, in order to stabilize the count, summands that are responsible for a mass force in the equation (1) and a thermocapillary force in the boundary condition (5) were additionally multiplied by a specially pre-defined function $f(t)$:

$$f(t) = \frac{1}{2}\left(erf\left(\frac{t - 10000}{2000}\right) + 1\right). \qquad (8)$$

Using this function makes it possible to omit effects related to a phase transition in this problem. Its kind was selected so that the thermal conduction problem was exclusively solved at the initial moments of time and only after continuously heating up all the all the areas the convective mechanisms were „included".

Results of simulation for the selected values of evolution parameters of the temperature and the rate are shown in Fig. 3. As shown by the calculations, heating of the reactor resulted in origination of the stationary flow that

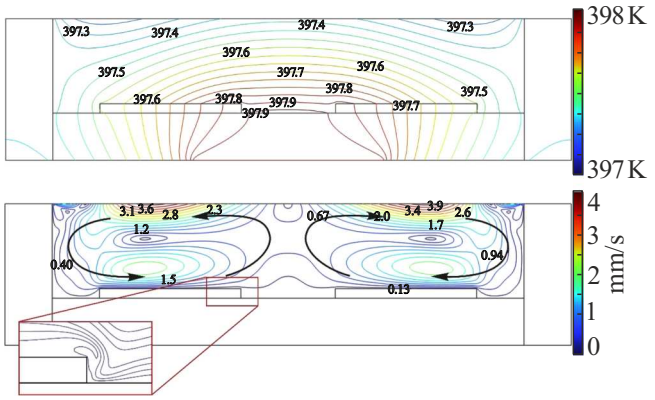



**Figure 3.** Field of the temperature (above) and the rate (below) in case of solving the problem without a fixing mask.

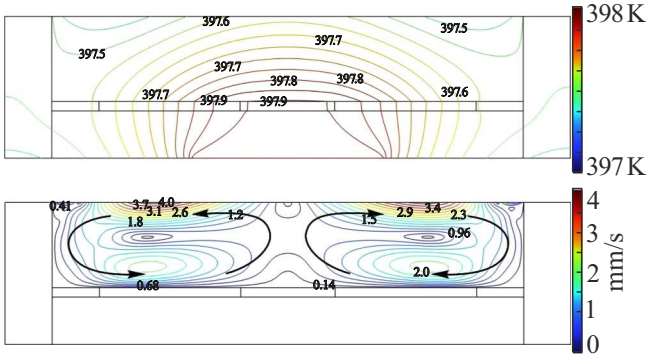



**Figure 4.** Field of the temperature (above) and the rate (below) in case of solving the problem with the fixing mask. The arrows mark a direction of the main flow.

was symmetrical relative to the center. Despite a small temperature difference, the rate of convective transfer of the benzoic acid can be up to $\sim 4\,\text{mm/s}$ at the free boundary.

Special attention should be paid to the shape of the flow near butt-end facets of the crystal. A bottom profile significantly affects a process of formation of small vortices, which can nucleate in an area in front of the crystals or in a cocurrent trail behind the samples. The problem was solved taking into account the fixing mask to show that its presence almost unaffected intensity of convective mass transfer and the kind of the main flow (Fig. 4). However, in case of a more even profile of the bottom the flow near protonated plates becomes more uniform and the system does not include vortices near the lithium niobate crystals. A shape and size of large-scale vortices are determined by the rate of the main flow, which depends on a value of the applied temperature gradient. In case of the small temperature drops, a weak creeping flow is formed and by onflowing to the sample it more heavily washes a crystal part that is nearer to a fore front of the flow. During formation of intense convection, when a shear stress at the sample boundaries exceeds a certain critical value, the melt

flows catch up and take away reaction product the more the higher flow rate.

It is important to note that the values of the temperature inside the benzoic acid melt, which are obtained in the count, differ from the values detected by the thermocouples during the experiment. Thus, the temperature difference per the layer of the benzoic acid melt is much higher in the experiment, thereby making convective transfer more intense than that obtained during numerical simulation. It shall result in much higher rates of convective transfer. Along with the cylindrical geometry of the reactor, these complicating factors will result in significant three-dimensionality of the flow. Likewise, this flow can no longer be considered to be a creeping one [53] and its description will require improving the system of equations (1)–(4). Moreover, in case of large temperature differences, the flow can lose stability and stationarity [54], but at the same time, with high supercriticalities the melt will homogenize in the system more intensely.

It was found when processing results of XDA and the method of prismatic input of the samples produced under different conditions of the full-scale experiment that depending on intensity of the convective flow the crystal surface formed the planar waveguides, which are different in the depth and the value of the increment of refractive index at the same pace of heating and cooling down the reactor as well as at the same time of holding the system for 2 h at the average temperature of 463 K. In this case, the process can be estimated by the value of $\delta$ only when comparing the samples with the same $\Delta n_e$, which is difficult when there is a large variety of the produced waveguides. Calculating an area under a curve of distribution of the increment of unusual beam's refractive index will neither provide a comprehensive picture, since this magnitude can widely vary when annealing the samples [55]. In our situation, this value varied from 5 % to 30 % from sample to sample before and after the annealing procedure. Therefore, it was decided to estimate a degree of the effect of the convective flow on the protonation process by calculating a number of protons $N$, which replace the lithium ions in the lithium niobate crystal during proton exchange. According to conclusions given in the study [26], when annealing in the dry atmosphere this magnitude shall be preserved in the sample, since the ions $H^+$ are just redistributed along the depth of the waveguide layer.

The number of protons in a volume under a waveguide's unit area of 1 $cm^2$ was calculated by the formula

$$N = \frac{\tilde{\rho} V C}{M} \cdot N_A, \tag{9}$$

where $N_A$ is the Avogadro's number, $\tilde{\rho}$ is a density of the waveguide, $V$ is a volume of the waveguide, $M$ is a molar mass of the solid solution $H_x Li_{1-x} NbO_3$ with the proton concentration C in the waveguide. In order to estimate $N$ in the first approximation, we neglect variation of the density of the waveguide relative to the initial value $\tilde{\rho} = 4700\ kg/m^3$ of the lithium niobate crystal [52]. Knowing $\Delta n_e$ by the results of the prismatic input measurements and using the graph of the dependence of the increment of refractive index on the proton concentration in the waveguide, which is given in the study [26], we determine the value of $C$.

It was shown by analyzing the graphs of the dependence of relative strain of the crystal lattice on displacement to the peaks and comparing the results with the structure-phase diagram of the proton-exchange waveguide layers [26] that after proton exchange the crystal surface formed the waveguides containing $\beta_1$- and $\beta_2$-phases. Estimation of the area under the curve $I/I_{\max}$ on strain $\varepsilon$ for each of the phases made it possible to determine that in the crystals of the $X$-transect approximately 45 % of the total depth of the waveguide was occupied by the $\beta_1$-phase, so was 55 % thereof in the $Z$-transect, whereas 55 % and 45 % of the waveguide depth in the $X$- and $Z$-transect respectively was allocated for the $\beta_2$-phase. A phase volume ratio was also taken into account when calculating the number of protons, which was done for post-annealed crystals as well. The results of calculation of $N$ on the applied temperature difference are shown in Fig. 5.

It is clear from the graphs that with the temperature drop per a unit length $\sim 1.5$ K/cm the number of protons penetrating the crystal during protonation obviously decreases. This effect can be explained as follows. Under effect of the washing flux, by removing lithium ions from a subsurface layer, the flow brings in a fresh reagent — pure benzoic acid, whose protons start actively penetrating into the crystal with intensity that is comparable with the initial proton-exchange stages, thereby forming the waveguide.

As demonstrated in the study [56], the free-proton concentration within the temperature interval 413–473 K in the benzoic acid melt is quite low, since a degree of dissociation of its molecules is small. With the low free-proton concentration in the acid melt, more probable is a mechanism of proton exchange by means of dissociative adsorption of the benzoic acid molecules with generation of participating protons directly on the surface on lithium niobate. In this scenario, locations near the crystal surface form an ion boundary layer made up by lithium ions and benzoate ions, which form the lithium benzoate impurity by recombining. When accumulating near the crystal surface, this impurity complicates adsorption and dissociation of the acid molecules, thereby resulting in an increase of activation energy. Presence of hydrodynamic fluxes makes it possible to divert the lithium ions and the benzoate ions from the lithium niobate surface and to bring the reagent molecules thereto. The low free-proton concentration in the acid melt will not result in their significant stratification by the density, whereas presence of intense mixing of the subsurface layers will just increase homogenization of the melt, which will result in leveling of the impurity concentration across the volume.

At first sight, the more intense the flux, the more protons shall enter the sample volume. However, with the high surface proton concentrations in the surface layer of the waveguide diffusion does not have enough time to transfer

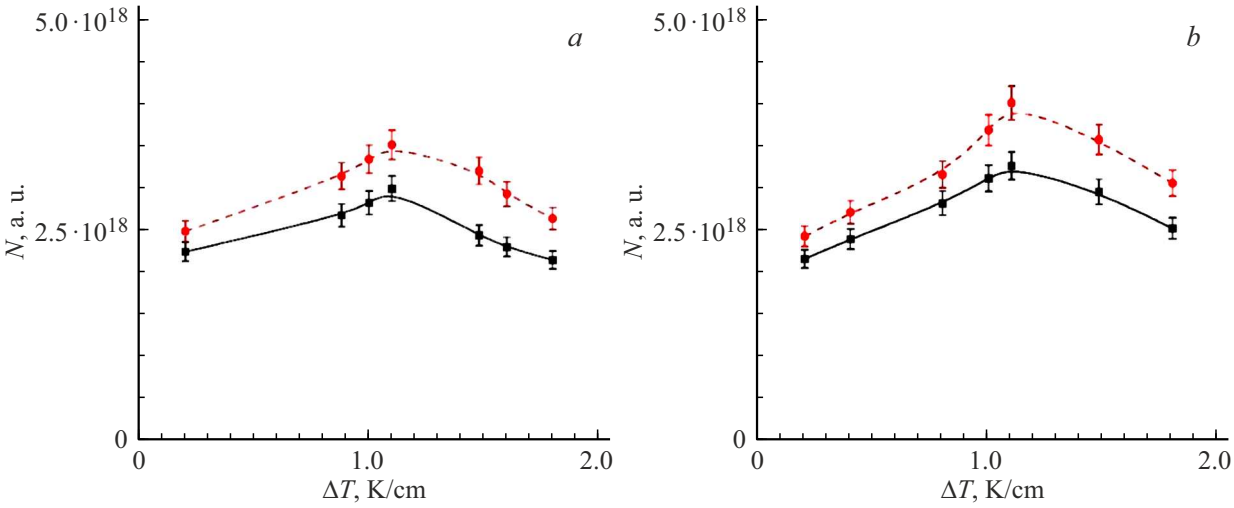



**Figure 5.** Number of protons that penetrated the crystal in a dependence on the temperature difference and are calculated after proton exchange (the solid curve) and after five-hour annealing at the temperature of 643 K (the dashed curve): *a* — *X*-transect, *b* — *Z*-transect.

the hydrogen ions deep into the crystal. The surface crystal layer with the increased proton concentration can result in formation of an electric field that prevents adsorption of new acid molecules. Another one of possible mechanisms of reduction of the proton exchange rate with intense fluxes in the system is reverse adsorption of lithium ions on the crystal surface to vacant locations still unoccupied by the hydrogen ions.

This result indirectly indicates that during proton exchange, there is possibly a layer being formed above the crystal surface within the benzoic acid volume, which has a high lithium-ion concentration and whose thickness can be controlled by means of the convective fluxes. At the same time, the melt-source-crystal system forms a certain balance for a rate of penetration of hydrogen protons into the sample and their diffusion drift into the crystal volume. It is assumed that in the performed experiments the characteristics of the layer above the crystal surface change, thereby resulting in variation of the proton exchange rate. The demonstrated effect of proton exchange acceleration with presence of thermogravitational convection can be used for reducing a process cycle time when producing the waveguides with characteristics that are identical to the waveguides produced as a result of proton exchange in the thermal chambers. In this case, the time and the post-annealing temperature mode will be the same, since the proton penetration depth after proton exchange will be the same for the waveguides with equal $\Delta n_e$ and $\delta$. Presence of thermogravitational convection makes it possible to reduce the first stage time — protonation, without changing the post-annealing time when producing the identical waveguides. Besides, leveling of the lithium-ion concentration within the melt volume can be useful during soft proton exchange, whose duration is quite significant and requires high temperatures [57,58], or during high-temperature proton exchange [59].

The observed increase of the number of proton after annealing is most likely related to inaccuracy of determination of the proton concentration in the waveguide by a graph given in the study [26]. A divergence of the curves in Fig. 5, which demonstrate the number of protons in the waveguide before and after annealing can be also affected by an error of determination of the depth of the proton exchange layer, wherein the dependence of the increment of unusual beam's refractive index on the concentration did not take into account presence of the $\beta_1$- and $\beta_2$-phases in the crystal in the first approximation when finding it.

Two pairs of the samples of the *X*- and *Z*-transects, which are produced during proton exchange in the thermal chamber with holding at the temperature of 463 K for 2 h as well as with availability of the source of the constant heat-release density when holding the crystals for 1 h with the temperature drop of 2.0 K/cm were compared to show that in terms of the magnitude $\Delta n_e(0)$ $\delta$ and $N$ the waveguides had similar values (see Table). It can be concluded from the Table data that presence of thermogravitational convection made it possible to accelerate the protonation process relative to the process in the thermal chamber.

The characteristics of the samples after annealing at the temperature of 643 K were studied to show that completely transforming the waveguides on the samples of the *X*-transect, which were produced when using the source of the constant heat-release density, from the $\beta_2$- into $\alpha$-phase requires 7 to 10 h versus 5 h for the waveguides produced on the samples of the *Z*-transect. Subsequent disappearance of intermediate phases during annealing results in formation of the waveguides with $\Delta n_e \sim 0.03$ and the depth of about 9 $\mu$m. It was found when comparing the number of protons $N$ that in the samples of the *X*-transect a value thereof exceeded the value of $N$ for the crystals of the *Z*-transect approximately in 1.5 times. This result also agrees with a conclusion that the structure of the *X*-transect is more

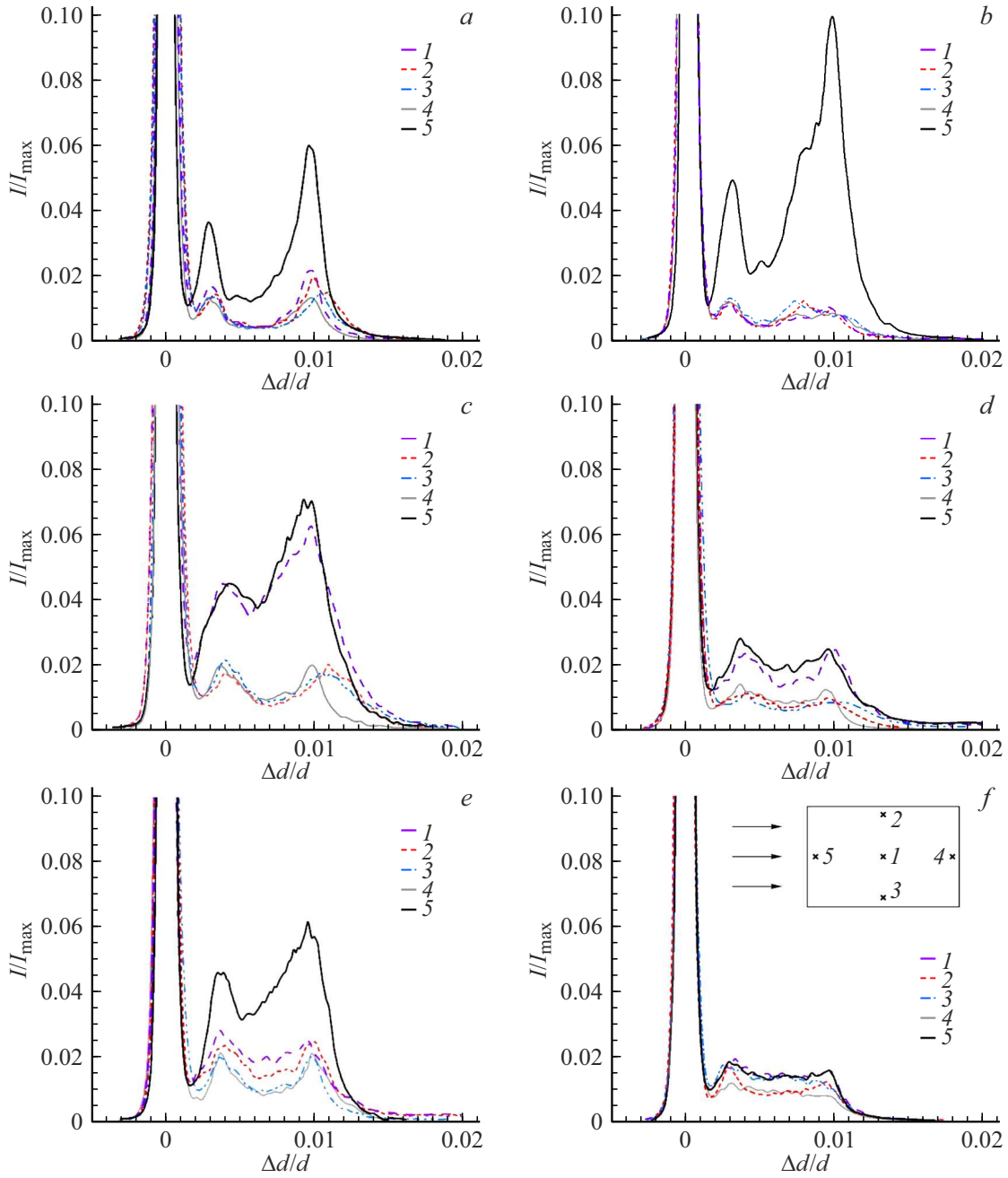



**Figure 6.** Dependence of normalized integral intensity on the value of strain on the lithium niobate crystals of the *X*-transect, which is determined after proton exchange without (on the left) and with (on the right) the fixing mask. The temperature drop in the reactor, K/cm: *a*, *b* — 0.5; *c*, *d* — 1; *e*, *f* — 1.4.

permeable for moving ions of lithium and hydrogen [60], thereby resulting in higher efficiency of proton exchange in the samples of the *X*-transect.

Results of determining normalized integral intensity on the value of strain, which is detected after proton exchange in five points on the surface of the samples for the crystals of the *X*-transect, which are produced at the various conditions of the experiment, are shown in Fig. 6. Similar dynamics is shown by the waveguides produced on the crystals of the *Z*-transect, but with a smaller variation of the magnitude $I/I_{max}$. The graphs $I/I_{max}$ on $\varepsilon$ in Fig. 6, *a*, *b* correspond to a case of proton exchange in the thermal chamber without (Fig. 6, *a*) and with fixation of the samples (Fig. 6, *b*). It is clear from the data presented that in a point on one of the side facets of the crystal (the solid curve) a higher value of integral intensity of the beam is detected than in a point in the sample center — the curve *1* and in a point at the distance of 2 mm from the edge in the center of other three facets — the curves *2*–*4*.

Increment of refractive index on the surface $\Delta n_e(0)$, the waveguide depth $\delta$, [$\mu$m], the number of protons in the waveguide $N$, [a. u.]

| Transect | Exposure time $h$, $\Delta T$ K/cm | After proton exchange | | | After annealing 5 h, $T = 643$ K | | |
|---|---|---|---|---|---|---|---|
| | | $\Delta n_e(0) \pm 0.0002$ | $\delta$ | $N \cdot 10^{18}$ | $\Delta n_e(0) \pm 0.0002$ | $\delta$ | $N \cdot 10^{18}$ |
| $X$ | 1, 2.0 | 0.1174 | 1.8 | 1.9 | 0.0353 | 7.1 | 2.3 |
| | 2, 0.2 | 0.1166 | 1.9 | 2.0 | 0.0383 | 6.9 | 2.4 |
| $Z$ | 1, 2.0 | 0.1162 | 1.4 | 1.5 | 0.0322 | 7.9 | 2.1 |
| | 2, 0.2 | 0.1172 | 1.4 | 1.5 | 0.0318 | 8.0 | 2.0 |

Presence of the fixing mask amplified the effect of heterogeneous protonation in the said point, simultaneously reducing a difference between readings of the other areas (Fig. 6, *b*). Presence of the thermocouples during the full-scale experiment made it possible to explain a cause of a difference in the values of $I/I_{\max}$, which are determined on the surface of one sample. Thus, during proton exchange in the thermal chamber the thermocouples input into the reactor were used to record the temperature drop from 0.1 to 0.25 K/cm in a dependence on a reactor position relative to the system center after the system reached the operating temperature of 463 K. The data from the thermocouples measuring the air temperature inside the chamber were analyzed to show that after heating up the various areas between furnace walls exhibit a temperature value divergence of about 5 K. It is assumed that the volume temperature gradient in the thermal chamber is so small that convective flows shall not be formed in the reactors during proton exchange. In the full-scale experiment, air was heated in the thermal chamber by thermal elements in its side walls. Additional mixing of an air volume was not designed. Presence of temperature heterogeneity in the air environment can result in nonuniform heating of the reactor and formation of weak thermogravitational convection inside the benzoic acid melt [38,39,50]. Comparison of a convective flux pattern and positions of the points, in which integral intensity was measured, is schematically shown in the insert of Fig. 6, *f*. The point, in which the highest value of $I/I_{\max}$ was recorded, was on a crystal facet that was the nearest relative to the onflowing flux. The obtained experimental data well agree with the conclusions made during numerical solution of the simulation problem that the weak creeping flow onflowing to the sample more heavily washed the crystal part that was nearer to the fore front of the flux.

With the more intense flow washing the samples, a case of proton exchange using the heat source of the constant heat-release density exhibited the difference in the value of $I/I_{\max}$ already for a larger number of the areas (Fig. 6, *c*, *e*). Unlike the case of proton exchange in the thermal chamber, on the contrary, using the fixing mask allowed neutralizing this effect. It also agrees with a conclusion that bottom planarity results in the more uniform protonation process, since the system has more intense mixing of the melt and lacks vortices near the crystals at the same time.

## Conclusion

We note in conclusion that despite a fine-tuned process of manufacturing the planar waveguides in the lithium niobate crystals by the proton-exchange method, this technological process still has multiple physical-chemical effects that require explanation. Thus, an installation was created in the study to observe dynamics of the temperature increase inside the reactor in real time, thereby enabling to correct a proton-exchange program when conditions of the process cycle were replaced as well as to trace a process of formation of the convective fluxes within the volume of the benzoic acid melt when the bottom and the walls of the reactor were inhomogeneously heated. The experimental studies that agree with the results of solution of the simulation problem indirectly confirm that near the crystal surface there is an ion boundary layer that was theoretically predicted before, whose formation directly affects the optical characteristics of the produced waveguides. The results of XDA and the method of prismatic input of the waveguides produced at the various modes are analyzed to indicate a positive effect of convection on the rate of exchange of lithium ions with benzoic acid protons. The obtained results make it possible to extend understanding of the mechanisms that play a big role in the proton-exchange reaction and to propose additional capabilities for its control and intensification.

### Acknowledgments

The study has used the proton-exchange reactor AN-0034 manufactured by LLC „Kontsept-Lab“ (Moscow).

### Funding

The study was supported financially by the Russian Science Foundation and Perm Krai (grant №. 24-29-20277).

### Conflict of interest

The authors declare that they have no conflict of interest.

## References


[1] H. Shu, L. Chang, Y. Tao, B. Shen, W. Xie, M. Jin, A. Netherton, Z. Tao, X. Zhang, R. Chen, B. Bai, J. Qin, S. Yu, X. Wang, J. E. Bowers. Nature, **605**, 457 (2022). DOI: 10.1038/s41586-022-04579-3

[2] E.L. Wooten, K.M. Kissa, A. Yi-Yan, E.J. Murphy, D.A. Lafaw, P.F. Hallemeier, D. Maack, D.V. Attanasio, D.J. Fritz, G.J. McBrien, D.E. Bossi. IEEE J. Selected Topics in Quant. Electron., **6** (1), 69 (2000). DOI: 10.1109/2944.826874

[3] D. Zhu, L. Shao, M. Yu, R. Cheng, B. Desiatov, C.J. Xin, Y. Hu, J. Holzgrafe, S. Ghosh, A. Shams-Ansari, E. Puma, N. Sinclair, C. Reimer, M. Zhang, M. Loncar. Adv. Opt. Photon, **13**, 242 (2021). DOI: 10.1364/AOP.411024

[4] S.S. Sun, L.R. Dalton. *Introduction to Organic Electronic and Optoelectronic Materials and Devices* (CRC press, Boca Raton, 2008), DOI: 10.1201/9781420009194

[5] T. Kawanishi. *Electro-Optic Modulation for Photonic Networks* (Springer, Switzerland, 2022), DOI: 10.1007/978-3-030-86720-1

[6] T. Tamir. *Integrated Optics. Topics in Applied Physics* (Springer Berlin, Heidelberg, 1975), DOI: 10.1007/978-3-662-43208-2

[7] R.K. Gangwar, S. Kumari, A.K. Pathak, S.D. Gutlapalli, M.C. Meena. Optics, **4**, 171 (2023). DOI: 10.3390/opt4010013

[8] R. Yin, Q. Huang, H. Yang, L. Lu, L. Cao, W. Ji, S. Jiang, Y. Luo, F. Liu, J. Sun, X. Yin, X.Su. Measurement, **183**, 109781 (2021). DOI: 10.1016/j.measurement.2021.109781

[9] V.M.N. Passaro, F. Dell'Olio, F. De Leonardis. Prog. Quant. Electron., **30** (2–3), 45 (2006). DOI: 10.1016/j.pquantelec.2006.08.001

[10] Z. Ye, H. Zhang, F. Shi, J. Fu, B. Wang, X. Gao, Y. Wang. Opt. Lett., **48**, 5659 (2023). DOI: 10.1364/OL.506448

[11] S. Abreu, I. Boikov, M. Goldmann, T. Jonuzi, A. Lupo, S. Masaad, L. Nguyen, E. Picco, G. Pourcel, A. Skalli, L. Talandier, B. Vettelschoss, E.A. Vlieg, A. Argyris, P. Bienstman, D. Brunner, J. Dambre, L. Daudet, J.D. Domenech, I. Fischer, F. Horst, S. Massar, C.R. Mirasso, B.J. Offrein, A. Rossi, M.C. Soriano, S. Sygletos, S.K. Turitsyn. Rev. Phys., **12**, 100093 (2024). DOI: 10.1016/j.revip.2024.100093

[12] Kh. Rissel, I. Ruge. *Ionnaya implantatsiya* (Nauka, M., 1983). [Per. s nem.: H. Ryssel, I. Ruge. *Ionenimplantation* (B.G. Teubner, Stuttgart, 1978), (in Russian). DOI: 10.1007/978-3-663-05668-3]

[13] V.P. Red'ko, O.D. Shlyakhtichev. Pis'ma v ZhTF, **4** (23), 1414 (1978) (in Russian).

[14] E.G. Guk, A.V. Kamanin, N.M. Shmidt, V.B. Shuman, T.A. Yurre. Semiconductors, **33** (3), 265 (1999).

[15] V.N. Ivanov, V.A. Nikitin, E.P. Nikitina, N.A. Yakovenko. ZhTF, (in Russian). **53** (10), 2088 (1983).

[16] F.G. Helfferich. *Ion exchange* (Dover Publications, NY., 1995)

[17] F.C. Nachod, J. Schubert. *Ion exchange technology* (Academic Press, NY., 1956)

[18] T. Volk, M. Wöhlecke. *Lithium Niobate: Defects, Photorefraction and Ferroelectric Switching* (Springer Berlin, Heidelberg, 2008), DOI: 10.1007/978-3-540-70766-0

[19] P. Mahmud, K.F. Supti, S.M. Choudhury. Opt. Express, **32**, 45786 (2024). DOI: 10.1364/OE.541271

[20] M. Kuneva. Int. J. Sci. Res. Sci. Technol., **2** (6), 40 (2016).

[21] S.T. Vohra, A.R. Mickelson, S.E. Asher. J. Appl. Phys., **66**, 5161 (1989). DOI: 10.1063/1.343751

[22] J.L. Jackel, C.E. Rice, J.J. Veselka. Appl. Phys. Lett., **41**, 607 (1982). DOI: 10.1063/1.93615

[23] Yu.N. Korkishko, V.A. Fedorov. J. Appl. Phys., **82** (3), 1010 (1997). DOI: 10.1063/1.365864

[24] Yu.N. Korkishko, V.A. Fedorov, S.M. Kostritskii. J. Appl. Phys., **84** (5), 2411 (1998). DOI: 10.1063/1.368437

[25] Yu.N. Korkishko, V.A. Fedorov. Crystallography Reports, **44** (2), 237 (1999).

[26] Yu.N. Korkishko, V.A. Fedorov. Tech. Phys., **44** (3), 265 (1999).

[27] M. Rottschalk, A. Rash, W. Karthe, J. Opt. Commun., **9**, 19 (1988). DOI: 10.1515/JOC.1988.9.1.19

[28] A. Loni, R.M. De La Rue, J.M. Winfield. J. Appl. Phys., **61** (1), 64 (1987). DOI: 10.1063/1.338801

[29] K.K. Wong. GEC J. Research, **3** (4), 243 (1985).

[30] A. Loni. *An experimental study of proton-exchanged lithium niobate optical waveguides* (PhD thesis, University of Glasgow, Glasgow, 1987)

[31] V.I. Kichigin, I.V. Petukhov, A.R. Kornilitsyn, S.S. Mushinsky. Condensed Matter Interphases, **24** (3), 315 (2022). DOI: 10.17308/kcmf.2022.24/9853

[32] M. De Micheli, J. Botineau, S. Neveu, P. Sibillot, D.B. Ostrowsky, M. Papuchon. Opt. Lett., **8** (2), 114 (1983). DOI: 10.1364/OL.8.000114

[33] V.I. Kichigin, I.V. Petukhov, S.S. Mushinsky, V.A. Oborin, A.M. Minkin, L.N. Malinina, D.I. Shevtsov, A.B. Volyntsev. *Proceedings of XIII International Conference and Seminar of Young Specialists on Micro/Nanotechnologies and Electron Devices* (Novosibirsk, Russia, 2012), p. 238. DOI: 10.1109/EDM.2012.6310225

[34] V.A. Demin, M.I. Petukhov. J. Siberian Federal Univer. Mathem. Phys., **18** (1), 100 (2025).

[35] V.A. Demin, M.I. Petukhov, R.S. Ponomarev, M. Kuneva. Langmuir, **39** (31), 10855 (2023). DOI: 10.1021/acs.langmuir.3c00957

[36] T. Sun, A.S. Teja. J. Chem. Eng. Data, **49** (6), 1843 (2004). DOI: 10.1021/je0497247

[37] R.E. Kirk-Othmer. *Encyclopedia of Chemical Technology* (Wiley, NY., 1991), v. 3, p. 625.

[38] G.Z. Gershuni, E.M. Zhukhovitskii. *Konvektivnaya ustoichivost' neszhimaemoi zhidkosti* (Nauka, M., 1972) (in Russian).

[39] G.Z. Gershuni, E.M. Zhukhovickii, A.A. Nepomnyashchii. *Ustoichivost' konvektivnykh techenii* (Nauka, M., 1989) (in Russian).

[40] A.I. Mizev, A.V. Shmyrov, A.I. Shmyrova. J. Fluid Mechanics, **939**, A24 (2022). DOI: 10.1017/jfm.2022.205

[41] A.V. Shmyrov, A.I. Mizev, V.A. Demin, M.I. Petukhov, D.A. Bratsun. J. Fluid Mechanics, **877**, 495 (2019). DOI: 10.1017/jfm.2019.613

[42] N.S. Bondareva, M.A. Sheremet. Teplofizika i aeromekhanika, (in Russian). **25** (4), 547 (2018).

[43] N.S. Bondareva, M.A. Sheremet. Teplofizika i aeromekhanika, (in Russian). **23** (4), 577 (2016).

[44] N.S. Bondareva, M.A. Sheremet. Intern. J. Heat Mass Transfer., **108**, 1057 (2017). DOI: 10.1016/j.ijheatmasstransfer.2016.12.108
[45] G.V. Kuznetsov, M.A. Sheremet. J. Appl. Mechan. Tech. Phys., **51**, 699 (2010). DOI: 10.1007/s10808-010-0090-2
[46] N.S. Bondareva, M.A. Sheremet. J. Magnetism Magnetic Mater., **419**, 476 (2016). DOI: 10.1016/j.jmmm.2016.06.050
[47] V.E. Zinov'ev. *Teplofizicheskie svoistva metallov pri vysokikh temperaturakh. Spravochnik* (Metallurgiya, M., 1989) (in Russian).
[48] E.A. Kolosovskii, D.V. Petrov, A.V. Tsarev. Sov. J. Quant. Electron., **11**, 1560 (1981). DOI: 10.1070/QE1981v011n12ABEH008650
[49] G.V. Kuznetsov, M.A. Sheremet. *Raznostnye methody resheniya zadach teploprovodnosti* (TPU, Tomsk, 2007) (in Russian).
[50] L.D. Landau, E.M. Lifshits. *Teoreticheskaya fizika. Gidrodinamika* (Fizmatlit, M., 1986) v. VI (in Russian).
[51] V.A. Demin, M.I. Petukhov, A.V. Shmyrov, A.I. Shmyrova. Interfacial Phenomena heat Transfer, **8** (3), 261 (2020). DOI: 10.1615/InterfacPhenomHeatTransfer.2020035273
[52] *Fomos-Materialy* electronic source. Available at: https://newpiezo.com/knowledge_base/crystals/niobat-litiya/ (date of access 28.04.2025)
[53] G. Shlikhting. *Teoriya pogranichnogo sloya* (Nauka, M., 1974) (in Russian).
[54] M.A. Sheremet. Teplofizika i aeromekhanika, **18** (3), 463 (2011) (in Russian).
[55] S.T. Vohra, A.R. Mickelson, S.E. Asher. J. Appl. Phys., **65**, 1429 (1989). DOI: 10.1063/1.343751
[56] V.I. Kichigin, I.V. Petukhov, S.S. Mushinskii, V.I. Karmanov, D.I. Shevtsov. Russ. J. Appl. Chem., **84** (12), 2060 (2011). DOI: 10.1134/S1070427211120081
[57] L. Chanvillard, P. Aschieri, P. Baldi, D.B. Ostrowsky, M. De Micheli, L. Huang, D.J. Bamford. Appl. Phys. Lett., **76** (9), 1089 (2000). DOI: 10.1063/1.125948
[58] Y.N. Korkishko, V.A. Fedorov, E.A. Baranov, M.V. Proyaeva, T.V. Morozova, F. Caccavale, F. Segato, C. Sada, S.M. Kostritskii. J. Opt. Society America A, **18** (5), 1186 (2001). DOI: 10.1364/JOSAA.18.001186
[59] Y.N. Korkishko, V.A. Fedorov, O.Y. Feoktistova. J. Lightwave Technol., **18**, 562 (2000). DOI: 10.1109/50.838131
[60] P. Nekvindova, J. Spirkova, J. Cervena, M. Budnar, A. Razpet, B. Zorko, P. Pelicon. Opt. Mater., **19**, 245 (2002). DOI: 10.1016/S0925-3467(01)00186-0

*Translated by M.Shevelev*